RevMexAA (Serie de Conferencias), **1**, 201-208 (1995)

POLARIZATION MODELS OF EMBEDDED PROTOSTARS

Barbara A. Whitney
Harvard-Smithsonian Center for Astrophysics
60 Garden St., Cambridge, MA 02138, USA

RESUMEN

Discuto el patrón de polarización que resulta de la dispersión de luz estelar central en una envoltura de polvo ópticamente gruesa en la *mayoría* de las líneas de visión. En objetos con regiones polares evacuadas, la luz dispersada que emerge está muy polarizada, con un mapa de polarización desviado del patrón que da una distribución de polvo esférica. Esta desviación resulta ser mayor a medida que la profundidad óptica en la línea de visión aumenta. Así, los patrones extremadamente asimétricos ocurren en las longitudes de onda más cortas (debido a la mayor opacidad del polvo), en las nubes más opacas y en las fuentes que se observan de canto.

ABSTRACT

I discuss the polarization which results from scattering of central starlight in a dusty envelope which is optically thick along *most* lines of sight. For objects with evacuated polar regions, the emergent scattered light is highly polarized, and the polarization map deviates from the centro-symmetric pattern expected of a spherical distribution of dust. The deviations become greater as the line-of-sight optical depth increases; thus, the extremely asymmetric patterns arise at the shortest wavelengths (due to higher dust opacity), in the most opaque clouds, and in the more edge-on sources.

Key words: **STARS: CIRCUMSTELLAR MATTER — STARS: PRE-MAIN-SEQUENCE — POLARIZATION — RADIATIVE TRANSFER**

1. INTRODUCTION

This paper describes polarization properties of a specific model, the Terebey, Shu, & Cassen (1984; hereafter TSC) free-fall collapse of a slowly rotating envelope onto a T Tauri star and disk (Shu 1977; TSC). At the early stages of collapse this picture is thought to describe the physical state of a Class I source, or protostar, with an age of about 10^5 years. Such a source emits most of its radiation in the far-infrared (IR) (10–200 μm) and usually drives a bipolar flow. I will describe the polarization that results from scattering of optical/near-IR radiation from the central T Tauri star in the surrounding disk and envelope.

I hope to show in this paper that the qualitative features in the polarization maps of the TSC collapse model arise for 2 reasons—high line-of-sight optical depth and relatively evacuated regions along other directions which allow light to escape (but only in limited directions). These same features appear in observed maps.

2. PHYSICAL MODEL

In the TSC collapse model, the cloud initially rotates as a solid body with angular velocity Ω, and has the density distribution, $\rho(r)$, of a singular isothermal sphere, $\rho \propto r^{-2}$. Collapse begins at the center, and information about the collapse proceeds out at the sound speed a (Shu 1977). We will consider the region of the envelope encompassed by the radius $R_0 = at$ where t is the time since the start of collapse. Inside this radius,

the envelope density can be described with two parameters, the infall rate, $\dot{M}$, and Ω (Ulrich 1976, Cassen & Moosman 1981). The infall rate is constant throughout the cloud, equal to $0.975a^3/G$ (Shu 1977). To describe the rotation rate, we will use the variable $R_c = (\Omega R_0^2)^2/(GM)$, which is the radius at which centrifugal force balances gravity. Material from the edge of the cloud, R_0, will fall onto a disk within a radius R_c. At all times in the collapse, half of the system mass is in the central star and half in the envelope (Shu 1977). Figure 1 of Whitney & Hartmann (1993) shows the density distribution for this cloud.

Our comparisons to observations so far have been of the Taurus molecular cloud, where the sound speed is about 0.2-0.3 km/s, giving an infall rate of $\sim 2-4\times10^{-6}M_\odot\ yr^{-1}$. The optical depth, proportional to the infall rate, is extremely large at optical wavelengths, ranging from ~20-200 at 0.55 μm, depending on the inclination. This is in good agreement with submillimeter estimates of extinction in envelopes around Class I sources (Barsony & Kenyon 1992). For a sound speed of $a = 0.25$ km/s, the expansion wave encompasses 1 solar mass (one-half in the central star) at a radius of $R_0 = 7100$ AU and at a time of 1.7×10^5 years.

The disk radii are generally estimated to be ≤ 100 AU (Adams, Emerson, & Fuller 1990; Beckwith et al. 1990). For the density structure of the disk we use the steady accretion disk in vertical hydrostatic equilibrium (Shakura & Sunyaev 1973; Lynden-Bell & Pringle 1974; Kenyon & Hartmann 1987). The disk is geometrically thin, with a height near the star only a fraction of a stellar radius, but optically thick.

Kenyon et al. (1993a) modelled the spectral energy distributions (SEDs) of the 22 Taurus protostars with infall rates of $2-4\times10^{-6}M_\odot\ yr^{-1}$ and $R_c \sim 50-300$ AU, in good agreement with the observational estimates (see also Adams, Lada, & Shu 1987). The models fit the observations over a wavelength range of 3 to 100 μm but fail to match the flux shortward of this. The Taurus protostars are a few to 10 magnitudes brighter at near-IR wavelengths than the SED models predict (and many more times this at optical wavelengths). Kenyon et al. (1993b) modelled the near-IR scattered light images of the Taurus protostars using a 2-D Monte Carlo code. We found that carving a narrow cavity into the TSC density distribution led to better comparison with the observations. The shape of the cavity is not important since the opening angle required is only about 10-20°. The cavity allows a small fraction of the stellar flux (a few percent) to escape through the polar regions and scatter into our line of sight. Even though this is a small fraction of the total emitted light, it is orders of magnitude greater than any direct light that can emerge from the opaque envelope.

3. MONTE CARLO MODELS

We use the Monte Carlo method to calculate scattering and polarization in the dusty disk+envelope. This allows us to include the asymmetric scattering properties of dust, and multiple scattering and polarization with relative ease. Our method is described in Whitney & Hartmann (1992, 1993), and Code & Whitney (1995). It is a standard method, in which we trace "photons" as they diffuse through a medium, following probabilistic interaction laws which are sampled using computer-generated random numbers. We emit a photon from the source into a random direction, sample an optical depth from the probability distribution $P(\tau) = e^{-\tau}$, integrate along the path until this optical depth is reached, and then sample for the next process, either absorption or scattering; alternatively, we can force the photon to scatter and weight its value by the albedo, which is the effective probability for scattering. If the photon scatters, we sample an angle of scatter from a rather complicated function which depends on incident polarization (Chandrasekhar 1960). There are different ways to sample from a probability distribution and the specific method affects the variance of the results. We choose to sample from the exact probability distribution using the rejection method which reduces the variance to a minimum, that of Poisson statistics. The programs collects exiting photons and bins by whatever quantities are desired: By binning in position of final scatter and angle, we have information we need to create images.

4. DUST PROPERTIES

The dust properties are useful to describe briefly because it gives insight into the wavelength dependence of the polarization maps I will show in the next section. We use the dust properties derived for the diffuse ISM. These may not be appropriate in dark clouds. However, the largest differences noticed so far between dark clouds and the diffuse ISM have been at ultraviolet wavelengths. Martin & Whittet (1990) found very little difference in the extinction properties in the near-IR between dark clouds and diffuse clouds, and argued that only the smaller grains, with radii less than 1 μm, vary from cloud to cloud.

The extinction properties of dust are well-known (see review by Mathis 1990), but the scattering properties are not as easily tested with observations, because the geometry of scattering must be known in order to separate the effects of the angular dependence of scattering from the albedo.

The parameters we use are 1) the asymmetry parameter g, used in the Henyey-Greenstein function to describe the angular dependence of the scattering. It ranges from 0 for isotropic scattering to 1 for 100% forward scattering; 2) the dust opacity, κ; 3) the albedo ω, which is the ratio of scattering opacity to total opacity; and 4) the maximum linear polarization, p_l. The polarization of dust is well-described by the Rayleigh function but is smaller by a factor p_l. Thus, while Thomson scattering has a maximum polarization of 100% (for a scattering angle of 90°), ISM dust has a maximum polarization of about 50% at optical wavelengths but approaches the Rayleigh value in the near-IR.

Table 1 lists the values we use based on models of the observed extinction properties, kindly provided by M. Wolfire. The models use the Mathis, Rumpl, & Nordsieck (1977) grain size distribution with optical constants from Draine (1985), and Draine & Lee (1984, 1987) The polarization values are from White (1979).

Table 1. Dust Properties
Theory

Band (λ [μm])	κ	ω	g	p_l
U(0.34)	426	0.51	0.48	0.26
B(0.44)	333	0.51	0.47	0.31
V(0.55)	253	0.51	0.44	0.43
R(0.73)	181	0.49	0.37	0.58
I(0.95)	122	0.46	0.29	0.70
J(1.25)	76	0.38	0.16	0.75
H(1.65)	45	0.29	0.06	0.87
K(2.20)	25	0.18	0.02	0.93

The things to note about the dust opacity are the variations with wavelength: In going from V-band to K, the opacity decreases by a factor of 10, the albedo goes down by a factor of 2, and the polarization goes up to almost 100%. In going from J to K, the major difference is that the opacity decreases by a factor of 3.

Consider what this does in our scattering models. At optical wavelengths, more light scatters (because of the higher albedo), with less polarization (because of low p_l and multiple scattering), but we may see none of the light if it cannot escape the envelope, due to the large optical depth (proportional to the opacity κ). In contrast, at K, not much light scatters (low albedo), but what does scatter has high polarization (large p_l and very little multiple scattering due to low albedo). In protostars, even at K, the optical depth of the envelope is large enough to extinct the direct unpolarized light, so that even with the low albedos, the emergent flux is dominated by scattered and highly polarized light. Thus, we expect that protostars may have very high polarizations in the near-IR if the scattering geometry is favorable.

5. POLARIZATION RESULTS

To describe the polarized image of an object we draw polarization vectors at each pixel, with the length denoting the magnitude of the polarization and the orientation showing the position angle. When light scatters off of a dust particle, the orientation of the resulting polarization—the position angle—is perpendicular to the plane of scattering; the magnitude of the polarization depends on the angle of scatter, the incident polarization, and p_l. Thus, if we view a source surrounded by a spherical distribution of scatterers, the polarization vectors will be perpendicular to the direction to the central source, and will form a circular pattern. Close to the star, our line of sight intercepts several scattering angles, so the polarization magnitude may decrease compared to further out in the cloud (where the scattering angles approach 90°). In addition, if the cloud is optically thin the point-spread-function of the bright, unpolarized central star will dominate the nearby scattered flux and the polarization will be tiny near the star. If the cloud is optically thick, multiple scattering will depolarize the light so the magnitude of the polarization vectors will be smaller; but the vectors will still form a circular pattern. If the cloud is extremely opaque and a tunnel is carved out, then radiation escapes only in one direction, giving only one scattering angle (or a narrow range). The position angle is perpendicular to this scattering angle. This is the situation we have in our protostar model. Most of the light escapes in the polar regions in tunnels which we presume are carved by jets.

Figures 1-3 show a set of models with $\dot{M} = 3.5 \times 10^{-6} M_\odot\, yr^{-1}$ and $R_c = 70$ AU, unless otherwise specified. Figure 1 shows this model at J and K wavelengths (1.25 μm and 2.2 μm) for an inclination of 78°. The image

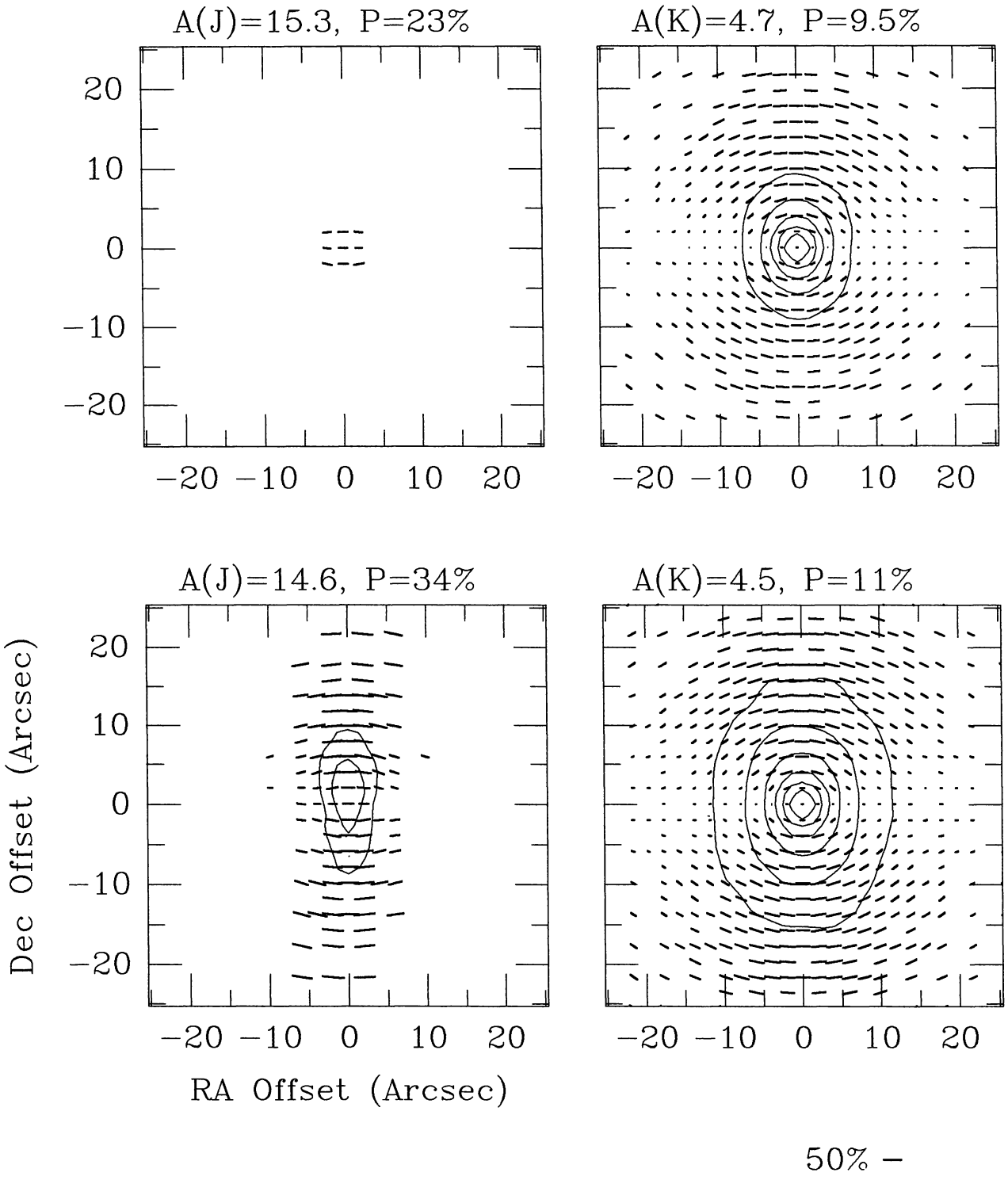

Fig. 1.— Top: Polarization maps at J (left) and K (right) for the TSC model with parameters $\dot{M} = 3.5 \times 10^{-6} M_{\odot}\, yr^{-1}$ and $R_c = 70$ AU. The inclination is 78°. Bottom: the same model with cavities in the polar regions, with 10° opening angles. A(J) and A(K) are the line-of-sight extinctions to the central source at J and K wavelengths respectively. The polarization integrated into 10″ apertures is oriented parallel to the disk plane with magnitudes listed above each plot.

dimensions are converted to arc seconds assuming a distance to the object of 140 pc (the distance to the Taurus molecular cloud). The map has been convolved with a Voigt point-spread-function (PSF) that has a FWHM of 2.4″ and $\gamma = 0.3$. This function fits a point source for the observations we presently compare to, obtained with the SQIID detector on the KPNO 1.3 m. The top images show the unmodified TSC model, and the bottom models have 10° holes carved out (measured from the polar axis—the full width subtends 20°). The labels above each image describe the extinction to the central source at the observed wavelength, and the polarization integrated into a 10″ diameter aperture. The position angle of the polarization in all of the models shown here is oriented parallel to the disk plane. In models with very low infall rate, the position angle is perpendicular to the disk plane as most scattering takes place in the equatorial region (the polarization still can be quite large in this case if the object is viewed very close to edge-on). The polarization maps are similar between the two models (top and bottom), though the integrated polarization is higher in the model with a hole. Note the high polarization vectors in the bottom left panel, greater than 50%. This image shows a striking pattern of nearly all parallel vectors. Most of the light has singly scattered in the polar cavity. With an optical depth through the equatorial region of greater than 14, less than 10^{-6} of the stellar flux can propagate through and scatter into our direction. This is the radiation that would give perpendicular vectors in the equatorial region. The small amount of light that is present in the equatorial region has 2 sources: it has scattered previously from the polar region (bypassing the thick envelope by jumping over it) and thus is multiply scattered, or it is a result of the PSF whose wings contribute flux from the polar regions. Both of these sources of light have position angle parallel to the disk plane.

At K, however, (right panels) the optical depth of the envelope drops by a factor of three; the amount of singly scattered light in the equatorial region is comparable to the combination of doubly scattered light and wings from the PSF. So in the equatorial region the polarizations cancel, giving near-0 polarization vectors.

The contours show the flux plotted at 1 magnitude intervals in brightness. The faintest contour has the same magnitude in all images, so the brighter objects will show more contours. The central source luminosity is the same in all images, and has the colors of an average T Tauri star + reprocessing disk (J-K = 1.2). Figure 1 shows that the TSC model with a narrow hole carved out is brighter by 1 magnitude at K and at least 2 magnitudes at J.

Figure 2 shows a model with a larger hole carved out, $\theta_H = 25°$, and at a lower inclination, $i = 60$. The J-band image has a lower extinction than those of Figure 1, but still shows high polarization, and a band of parallel vectors along the equator. In the K image, the extinction is low enough that the direct stellar flux begins to dominate the image. The polarization is lower everywhere because of the addition of unpolarized flux from the wings of the PSF. Note that the integrated polarization is much lower than the K-band images in Figure 1.

Figure 3 snows a set of K-band images. These have hole sizes of 10°, like that in Figure 1 at bottom right. The top 2 images show the effect of varying infall rate, which changes the optical depth through the envelope. The high infall rate image (top left) looks like the J image in Figure 1. The low-infall rate model shows the the bright central source starting to dominate. These images illustrate that the wavelength dependence of the polarization maps can be understood almost entirely as an optical depth effect. The J-band sees a more opaque envelope than the K-band. The bottom images in Figure 3 show the effect of varying the wings in the PSF. This model is the same as that in Figure 1, bottom right, but the γ function is changed from 0.3 to 0.15 (left) and 0.45 (right). This effect is most pronounced when the component of direct unpolarized light from the central source is comparable to or greater than the diffuse emission. The diffuse emission from these models *totals* about 1-3%, with only a small fraction of this in a given pixel so we require an extinction of 4-5 magnitudes to block the direct light. Even if the central source is blocked, but most of the flux comes from the central region, the wings of the PSF can cause this polarized flux to dominate over other regions, and this should be taken into account when examining polarization maps.

6. COMPARISON TO OBSERVATIONS

The polarization maps of several pre-main sequence objects have what is called a "polarization disk", in which the polarization clearly departs from a centrosymmetric pattern: The equatorial band contains parallel vectors usually of a smaller magnitude than the centrosymmetric vectors that are in the polar regions, and null vectors may lie at the outer regions of the equatorial band. Objects which exhibit this behavior include NGC 2261/R Mon (Warren-Smith, Draper & Scarrott 1987; Minchin et al. 1991), L1551 IRS 5 (Lenzen 1987), PV Cep (Gledhill, Warren-Smith, & Scarrott 1987), R and T Cr A (Ward-Thompson et al. 1985), Par 21 (Draper, Warren-Smith, & Scarrott 1985), and HL Tau (Gledhill & Scarrott 1989). A more detailed listing of polarization maps is given in Bastien & Ménard (1990).

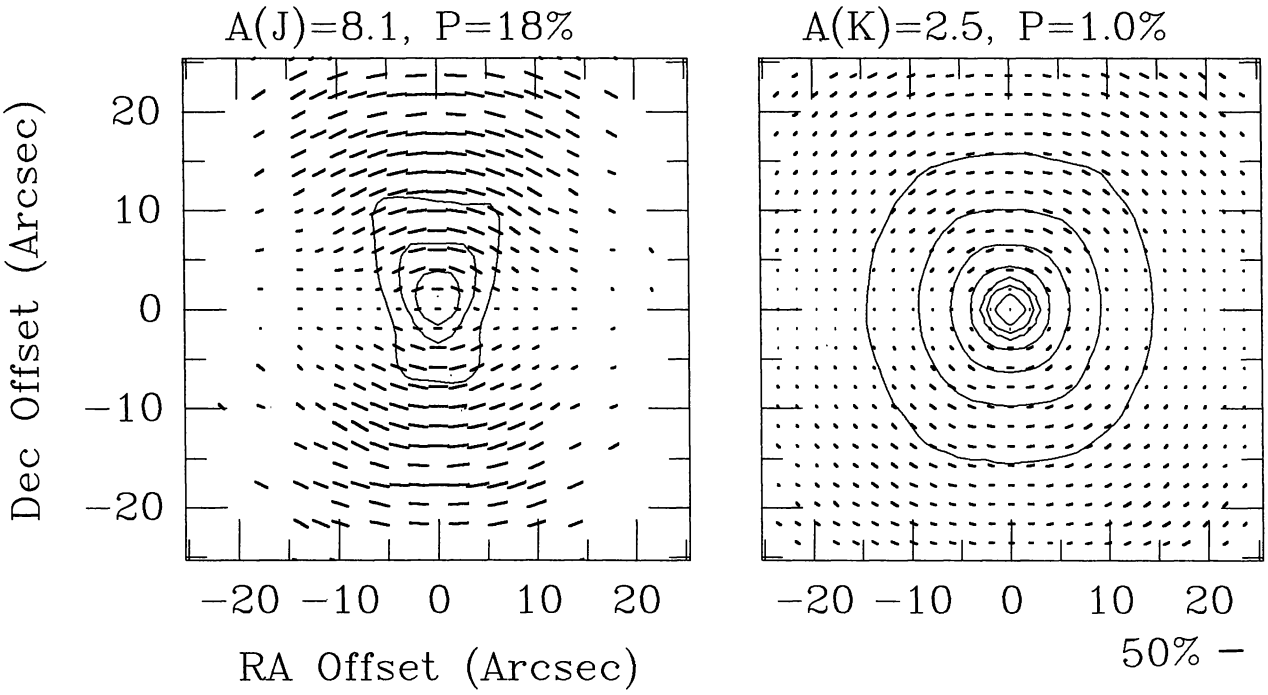

Fig. 2.— This has the same model parameters as in Figure 1 but the hole size is 25° and the inclination is 60°.

We find these patterns can be produced in the TSC density distribution. Other models also fit these patterns: Bastien & Ménard (1988, 1990) make polarization disks using large ($10^3 - 10^4$ AU radius) disks and optically thin envelopes in the polar regions. Gledhill (1991) can reproduce observed polarization maps with a central source with large polarization parallel to the disk plane surrounded by an optically thin envelope. However, most of these sources are known to have optically thick envelopes, so this model may not apply. Fischer, Henning, & Yorke (1994) simulate polarization maps of protostars using the density distribution from a hydrodynamic model of collapse including rotation. They vary dust properties and compute circular polarization due to multiple scattering. Their linear polarization maps agree with observed features, for the same reason as ours, because the geometry and optical depths are similar. In this meeting, Galli (1995) presented polarization maps for magnetic collapse (this volume), and Men'shchikov, Henning, & Fischer presented polarization models maps for HL Tau which use an optically thick spherical envelope with a conical hole carved out. With the exception of Gledhill's model, these models all include an optically thick line of sight to the source through a disk or envelope, and relatively evacuated polar regions.

Alternatively, Gething et al. (1982) and others (see Scarrott et al. 1990) suggest that the polarization maps characteristic of pre-main sequence stars may be caused by dichroic extinction from grains aligned in a toroidal magnetic field. Bastien & Ménard (1990) list several arguments against the aligned grain model. In addition to these, there is the problem that the envelopes may be too opaque for light to propagate through the equatorial regions and be anisotropically absorbed.

The models of Kenyon et al. (1993b) which fit the SEDs of the Taurus protostars make predictions for the polarizations of these sources. Integrated into 10″ apertures, the model polarizations range from a few percent up to 20% at K, 30% at H, and 40% at J. We recently obtained polarimetry of all the sources and measured polarizations up to 20% at K, 30% at H, but only 25% at J. We may have suffered a selection effect at J, since the most highly polarized sources are likely to be edge-on and therefore the most faint, and we could not measure the faintest sources at J. We obtained polarization maps of the brightest Class I sources in the Taurus-Aurigae molecular cloud. Nearly all show parallel vectors in the midplane. If the models do represent real protostars, the observations will narrow our range of envelope parameters, favoring the low end of R_c and the high end of $\dot{M}$. These results will be presented in a forthcoming paper.

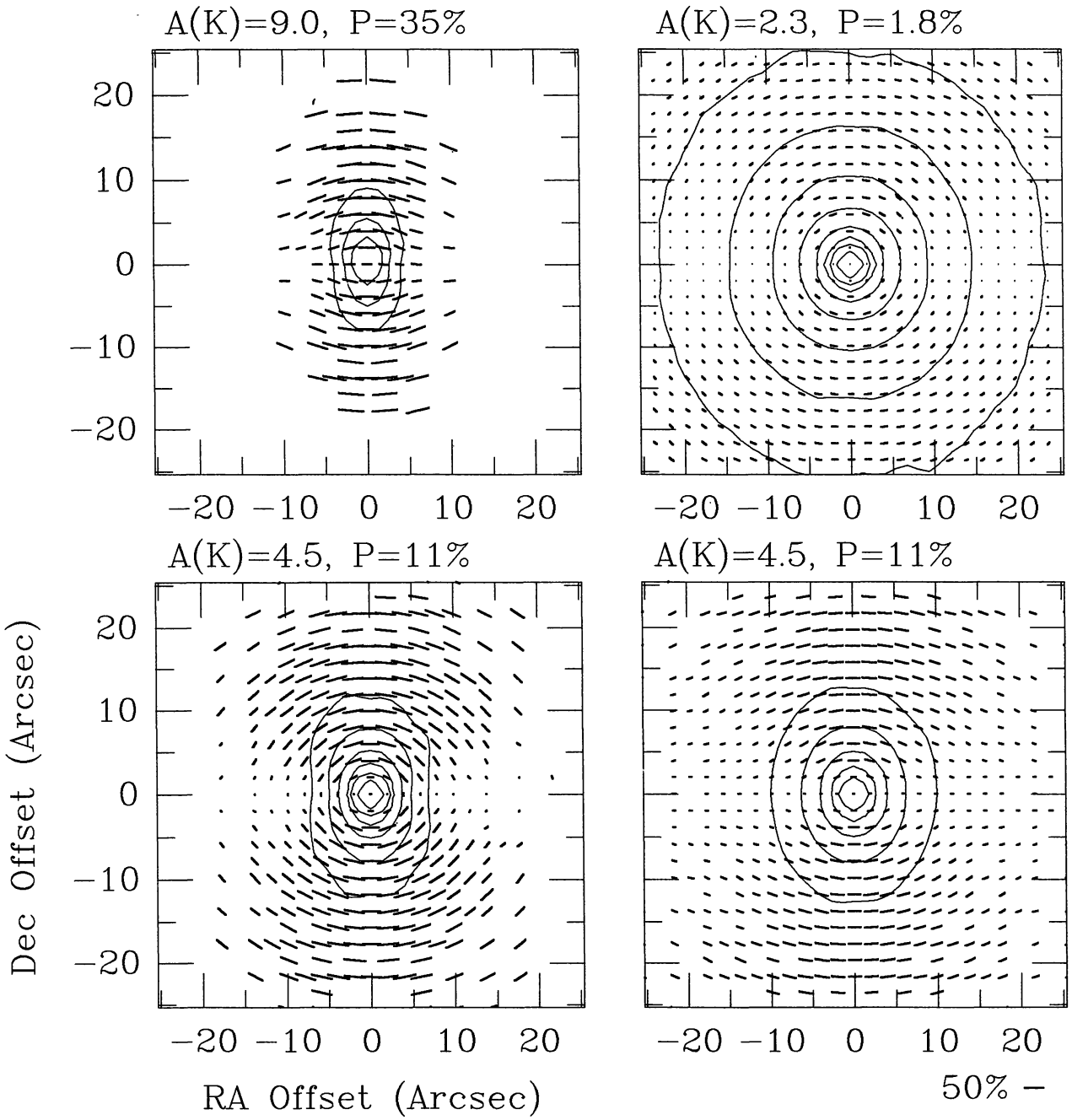

Fig. 3.— The top two panels show how the K images change as the infall rate varies from $\dot{M} = 1.75 \times 10^{-6}$ to $\dot{M} = 7 \times 10^{-6}$. The other model parameters are the same as the image at bottom-right in Figure 1. The bottom two panels show the effect of changing the PSF of the convolved point source. The parameter of the Voigt function which determines the extent of the wings is γ which is set to 0.15 in the left panel, and 0.45 at right. Compare this to the K image in Figure 1 (bottom-right) which has $\gamma = 0.3$.

7. FINAL POINTS

Our scattering models applied to protostars, using the rotating infall model of TSC, predict large polarizations in the near-IR. This suggests that near-IR polarization measurements of star forming regions could be used to find protostars. The model polarization maps resemble those of observed young stellar objects.

The scattering models for protostars allow about 1-2% of the light to escape into your line-of-sight at J-H-K wavelengths. To see high polarization, therefore, the envelope must extinct the direct stellar light by at least 4-5 magnitudes to allow the scattered flux to dominate. For sources with high polarization at K, this implies optical extinctions of greater than 100 at 0.55 μm.

If protostars do have narrow cavities, the small fraction that are viewed closer to pole-on will not be classified as a protostar using the standard definitions. These sources will have optically bright T Tauri stars and low polarization. At intermediate inclinations, the source would have low K-polarization but high optical polarization. One such example may be HL Tau. An example of a pole-on source may be T Tau. Calvet et al. (1994) modelled the SEDs of T Tau and HL Tau using the TSC envelope with a hole viewed closer to pole-on. These sources, and other "flat-spectrum sources" may be younger than previously thought.

REFERENCES

Adams, F. C., Emerson, J. P., & Fuller, G. A. 1990, ApJ, 357, 606
Adams, F. C., Lada, C. J., & Shu, F. H. 1987, ApJ, 312, 788
Barsony, M., & Kenyon, S. J. 1992, ApJ, 384, L53
Bastien, P., & Ménard, F. 1988, ApJ, 326, 334
____ 1990, ApJ, 364, 232
Beckwith, S. V. W., Sargent, A. I., Chini, R., & Güsten, R. 1990, AJ, 99, 924
Calvet, N., Hartmann, L., Kenyon, S. J., & Whitney, B. A. 1994, ApJ, 434, 330.
Cassen, P., & Moosman, A. 1981, Icarus, 48, 353
Chandrasekhar, S. 1960, in Radiative Transfer (New York: Dover).
Code, A. D., & Whitney, B. A. 1995, ApJ, in press
Draine, B. T. 1985, ApJS, 318, 485
Draine, B., & Lee, H.M. 1984, ApJ, 285, 89
Draine, B. T., & Lee, H. M. 1987, ApJ, 318, 485
Draper, P. W., Warren-Smith, R. F., & Scarrott, S. M. 1985, MNRAS, 216, 7p
Fischer, O., Henning, Th., & Yorke, H. W. 1994, A&A, 284, 187
Galli, D. 1995, in Disks, Outflows and Star Formation, ed. S. Lizano & J. M. Torrelles, RevMexAASC, 1, 179
Gething, M. R., Warren-Smith, R. F., Scarrott, S. M., & Bingham, R. G. 1982, MNRAS, 198, 881
Gledhill, T. M. 1991, MNRAS, 252, 138
Gledhill, T. M., & Scarrott, S. M. 1989, MNRAS, 236, 139
Gledhill, T. M., Warren-Smith, R. F., & Scarrott, S. M. 1987, MNRAS, 229, 643
Kenyon, S. J., & Hartmann, L. 1987, ApJ, 323, 714
Kenyon, S. J., Calvet, N., & Hartmann, L. 1993a, ApJ, 414, 676
Kenyon, S. J., Whitney, B. A., Gómez, M., & Hartmann, L. 1993b, ApJ, 414, 773
Lenzen, R. 1987, A&A, 173, 124
Lynden-Bell, D., & Pringle, J. E. 1974 MNRAS, 168, 603
Martin, P. G., & Whitett, D. C. B. 1990, ApJ, 357, 113
Mathis, J. S. 1990, ARA&A, 28, 37
Mathis, J. S., Rumpl, W., & Nordsieck, K. H. 1977, ApJ, 217, 425
Minchin, N. R., Hough, J. H., McCall, A., Aspin, C., Yamashita, T., & Burton, M. G. 1991, MNRAS, 249, 707
Scarrott, S. M., Gledhill, T. M., & Rolph, C. D. 1990, QJRAS, 31, 47
Shakura, N. I., & Sunyaev, R. A. 1973, A&A, 24, 337
Shu, F. H. 1977, ApJ, 214, 488
Terebey, S., Shu, F.H., & Cassen, P. 1984, ApJ, 286, 529 (TSC)
Ulrich, R. K. 1976, ApJ, 210, 377
Ward-Thompson, D., Warren-Smith, R. F., & Scarrott, S. M. 1985, MNRAS, 215, 537
Warren-Smith, R. F., Draper, P. W., & Scarrott, S. M. 1987, ApJ, 315, 500
White, R. L. 1979, ApJ, 229, 954
Whitney, B. A., & Hartmann, L. 1992, ApJ, 395, 529
Whitney, B. A., & Hartmann, L. 1993, ApJ, 402, 605